



Object-Based Analyses in FIJI/ImageJ to Measure Local RNA Translation Sites in Neurites in Response to A β 1-42 Oligomers

María Gamarra^{1,2}, Maite Blanco-Urrejola^{1,2,3}, Andreia F. R. Batista^{1,4,5}, Josune Imaz² and Jimena Baleriola^{1,3,6*}

¹ Achucarro Basque Center for Neuroscience, Leioa, Spain, ² Department of Neurosciences, Faculty of Medicine and Nursing, University of the Basque Country, Bilbao, Spain, ³ Department of Cell Biology and Histology, Faculty of Medicine and Nursing, University of the Basque Country, Leioa, Spain, ⁴ Life and Health Sciences Research Institute, School of Medicine, University of Minho, Braga, Portugal, ⁵ ICVS/3B's, PT Associate Laboratory, Universidade do Minho, Guimarães, Portugal, ⁶ IKERBASQUE Basque Foundation for Science, Bilbao, Spain

OPEN ACCESS

Edited by:

João O. Malva,
University of Coimbra, Portugal

Reviewed by:

Luisa Cortes,
University of Coimbra, Portugal
Ramiro Almeida,
University of Aveiro, Portugal

*Correspondence:

Jimena Baleriola
jimena.baleriola@achucarro.org

Specialty section:

This article was submitted to
Brain Imaging Methods,
a section of the journal
Frontiers in Neuroscience

Received: 19 December 2019

Accepted: 04 May 2020

Published: 03 June 2020

Citation:

Gamarra M, Blanco-Urrejola M, Batista AFR, Imaz J and Baleriola J (2020) Object-Based Analyses in FIJI/ImageJ to Measure Local RNA Translation Sites in Neurites in Response to A β 1-42 Oligomers. *Front. Neurosci.* 14:547. doi: 10.3389/fnins.2020.00547

Subcellular protein delivery is especially important in signal transduction and cell behavior, and is typically achieved by localization signals within the protein. However, protein delivery can also rely on localization of mRNAs that are translated at target sites. Although once considered heretical, RNA localization has proven to be highly conserved in eukaryotes. RNA localization and localized translation are especially relevant in polarized cells like neurons where neurites extend dozens to hundreds of centimeters away from the soma. Local translation confers dendrites and axons the capacity to respond to their environment in an acute manner without fully relying on somatic signals. The relevance of local protein synthesis in neuron development, maintenance and disease has not been fully acknowledged until recent years, partly due to the limited amount of locally produced proteins. For instance, in hippocampal neurons levels of newly synthesized somatic proteins can be more than 20–30 times greater than translation levels of neuritic proteins. Thus local translation events can be easily overlooked under the microscope. Here we describe an object-based analysis used to visualize and quantify local RNA translation sites in neurites. Newly synthesized proteins are tagged with puromycin and endogenous RNAs labeled with SYTO. After imaging, signals corresponding to neuritic RNAs and proteins are filtered with a Laplacian operator to enhance the edges. Resulting pixels are converted into objects and selected by automatic masking followed by signal smoothing. Objects corresponding to RNA or protein and colocalized objects (RNA and protein) are quantified along individual neurites. Colocalization between RNA and protein in neurites correspond to newly synthesized proteins arising from localized RNAs and represent localized translation sites. To test the validity of our analyses we have compared control neurons to A β 1–42-treated neurons. A β is involved in the pathology of Alzheimer's disease and was previously reported to induce local translation in axons and dendrites which in

turn contributes to the disease. We have observed that A β increases the synthesis of neuritic proteins as well as the fraction of translating RNAs in distal sites of the neurite, suggesting an induction of local protein synthesis. Our results thus confirm previous reports and validate our quantification method.

Keywords: local protein synthesis, RNA localization, neurites, fluorescence microscopy, FIJI/ImageJ analyses, colocalization analyses

INTRODUCTION

Among all cell types, neurons are the most morphologically complex. The nucleus is contained in a cell body or soma, from where several neurites emerge. Neuronal dendrites measure around ten millimeters and axons can reach one meter of length in vertebrates (Bannister and Larkman, 1995b). This extremely polarized morphology reflects the also polarized function of neurons. Whereas dendrites receive signals, the cell body processes them and axons are responsible for transmitting information to adjacent neurons. To maintain a proper function, each neuronal compartment needs to react temporally and spatially in an acute manner in order to rapidly adapt to changes in the environment. These implies that compartmentalized signaling events are required and therefore neuronal proteins must be asymmetrically distributed.

The origin of neuritic proteins (both dendritic and axonal) has been discussed for years. It was classically thought that proteins that support dendritic and axonal functions are synthesized in the soma and then transported to the target compartment at peripheral sites of the neuron. However, in the 19th century, the possibility of neurites, especially axons, producing their own proteins locally was already hypothesized (review in Bolton, 1901). This unconventional view of protein distribution to different neuronal compartments has been finally accepted by the scientific community. In order to synthesize proteins locally, messenger RNAs (mRNAs) and components of translational machinery must be transported to neurites. mRNAs are localized to dendrites and axons as part of ribonucleoprotein (RNPs) complexes in a translationally repressed state. Exogenous stimulus sensed by neurites influence the local translation machinery and mRNAs are released from RNPs complexes. Once associated to localized ribosomes, mRNAs are translated and proteins are synthesized independently from the soma and thus the endoplasmic reticulum (ER) (Jung et al., 2012).

The requirement of local intra-dendritic translation for nervous system plasticity has been extensively studied. Local translation in axons is involved in growth cone behavior, axonal pathfinding and maintenance, as well as in retrograde signaling (reviewed in Jung et al., 2014; Holt et al., 2019). More recently, it has been reported that adult axons are also able to respond to pathological insults by changing their local translome. In particular, after a nerve injury, mRNAs are locally translated and newly synthesized proteins contribute to axonal regeneration (Terenzio et al., 2018). Similarly, in the central nervous system (CNS) intra-axonal protein synthesis induced by A β _{1–42} oligomers, whose accumulation is central to Alzheimer's disease (AD), contributes to neurodegeneration (Baleriola et al.,

2014; Walker et al., 2018). Interestingly some authors have linked intra-dendritic translation and Tau mislocalization and hyperphosphorylation (Kobayashi et al., 2017; Li and Gotz, 2017). Thus, dysregulation of local protein synthesis might play a more relevant role in nervous system dysfunction than previously acknowledged.

AD is characterized by synaptic dysfunction during early stages (Palop and Mucke, 2010). Understanding dynamic early changes in the local proteome is in our view crucial to understand basic pathological mechanisms underlying AD and likely other neurological diseases. An accurate quantification of local translation foci, which is the aim of this study, might therefore give important clues to the extent to which changes in the local translome contribute to the disease. Currently the most frequently used techniques to detect local translation in neurons are FUNCAT (FLUorescent Non-Canonical Amino acid Tagging) and SUNSET (SURface SENSing of Translation). The first utilizes modified amino acids, such as azidohomoalanine, that get incorporated into the nascent polypeptide chain. The non-canonical amino acids are then tagged with a fluorophore in a cycloaddition reaction (Dieterich et al., 2010). SUNSET is based in the use of the antibiotic puromycin, which mimics an aminoacyl-transfer RNA (tRNA). Puromycin binds to the acceptor site of the ribosome during translation elongation leading to translation termination. The truncated puromycylated polypeptide can be detected by immunofluorescence using an anti-puromycin antibody (Schmidt et al., 2009). The fluorescence signal measured by both approaches is used as a readout of protein synthesis. Nevertheless, the low amount of locally produced proteins entails a limitation in the study of this phenomenon. For instance, our own results indicate that levels of newly synthesized neuritic proteins can be 20 to 30 times lower than somatic protein levels in unstimulated conditions. Thus, local translation sites in neurites can be easily overlooked when analyzing *de novo* synthesis by fluorescence microscopy. To overcome this situation, we have developed a simple method that helps visualize and quantify puromycin-positive sites in neurites by filtering and binarizing imaged cells using FIJI/ImageJ. Moreover, we have used a combination of RNA and protein staining techniques followed by object-based colocalization to detect sites of local RNA translation in neurons.

MATERIALS AND METHODS

Animals

All animal protocols followed the European directive 2010/63/EU and were approved by the UPV/EHU ethics committee.

Sprague-Dawley rats were bred in local facilities and embryonic brains were obtained from CO₂ euthanized pregnant rats.

Neuronal Cultures

Hippocampal neurons were prepared from embryonic day 18 rat embryos (E18) as described (Banker and Goslin, 1998). Briefly, hippocampi were dissected from embryonic brains and dissociated in TrypLE Express (Gibco, Thermo Fisher Scientific, Waltham MA, United States) for 10 min at 37°C. Cells were washed twice with Hank's balanced salt solution (HBSS, Gibco) and resuspended in plating medium containing 10% fetal bovine serum, 2 mM L-glutamine and 50 U.ml⁻¹ penicillin-streptomycin in Neurobasal (all from Gibco). Cells were homogenized with a pasteur pipette and centrifuged for 5 min at 800 rpm. Cells were resuspended in plating medium. Hippocampal neurons were cultured on poly-D-lysine-coated coverslips in 24-well plates at low density (35,000 cells/cm²), similar to previous reports in which newly synthesized proteins along individual neurites were visualized (Dieterich et al., 2010; Graber et al., 2013; Hafner et al., 2019). Cultures were maintained at 37°C in a 5% CO₂ humidified incubator. After 1 day *in vitro* (1 DIV) the medium was replaced with growth medium (1 × B27, 2 mM glutamine, and 50 U.ml⁻¹ penicillin-streptomycin in Neurobasal). To avoid the growth of glia, half of the medium was replaced with fresh medium containing 20 μM of 5-fluorodeoxyuridine and uridine (Sigma Aldrich, Merck, Darmstadt, Germany) every 3 days. Treatments were performed at 9–10 DIV.

Oligomeric Aβ Preparation and Treatments

Soluble oligomeric amyloid-β (Aβ_{1–42}) was prepared as previously described (Quintela-Lopez et al., 2019). Synthetic Aβ_{1–42} (Bachem, Bubendorf, Switzerland) was dissolved in hexafluoroisopropanol (HFIP, Sigma Aldrich) to 1 mM, aliquoted and dried. For oligomer formation, the peptides were resuspended in dry dimethylsulfoxide (DMSO; 5 mM, Sigma Aldrich) and Hams F-12 (PromoCell Labclinics, Barcelona, Spain) was added to adjust the final concentration to 100 μM. Peptides were incubated overnight at 4°C. Oligomerized Aβ was added to neurons at 9 DIV at a 3 μM concentration and incubated for 24 h. DMSO was used as vehicle control.

Puromycylation Assay

Puromycin is a tRNA analog, which is incorporated into the nascent polypeptide chain in a ribosome-catalyzed reaction. This technique allows the *in situ* detection of protein synthesis with an anti-puromycin antibody. At 10 DIV, DMSO- and Aβ-treated neurons were exposed to 2 μM puromycin (Sigma Aldrich) for 5–30 min as indicated. Control conditions with no puromycin received only fresh growth medium (vehicle). To verify that puromycin labels newly synthesized proteins, 40 μM of the translation inhibitor anisomycin (Sigma Aldrich) was co-incubated with puromycin. Cells were washed with cold PBS with 3 μg.ml⁻¹ digitonin (Sigma Aldrich) and fixed in 4% paraformaldehyde (PFA), 4% sucrose in PBS.

Immunocytochemistry

Neurons were fixed for 20 min at room temperature in 4% PFA, 4% sucrose in PBS. Cells were washed three times with PBS, permeabilized and blocked for 30 min in 3% BSA, 100 mM glycine and 0.25% Triton X-100. Next, samples were incubated overnight at 4°C with primary antibodies including mouse anti-puromycin (1:500, MABE343, Merck Millipore), rabbit and chicken anti-βIII tubulin (1:500, ab18207 and ab107216, respectively, Abcam, Cambridge, United Kingdom), rabbit anti-Tau (1:1000, ab32057, Abcam) and rabbit anti-calreticulin (1:500, ab92516, Abcam). After three PBS washes, cells were incubated for 1 hr at room temperature with fluorophore-conjugated secondary antibodies: anti-mouse Alexa Fluor 594 (1:200, A-11005, Invitrogen, Thermo Fisher Scientific), anti-rabbit Alexa Fluor 488 (1:200, A-21206, Invitrogen), anti-chicken DyLight 350 (1:200, SA5-10069, Invitrogen), anti-rabbit Alexa Fluor 647 (1:200, A-31573, Invitrogen) and anti-rabbit DyLight 405 (1:200, 611-146-002, Rockland Immunochemicals, Pottstown, PA, United States). Samples were washed three times with PBS and mounted with ProLong Gold antifade reagent (P-36930, Invitrogen). Whenever stated, a no-primary-antibody negative control was used.

To label endogenous RNAs neurons were washed once with cold PBS with 3 μg.ml⁻¹ digitonin (Sigma Aldrich), once with 50% methanol in PBS and fixed in cold 100% methanol for 5 min. Samples were rehydrated by washing them in 50% methanol in PBS once and in PBS three times. Following the standard immunocytochemistry procedure, cells were incubated for 20 min at room temperature with SYTO RNaselect green fluorescent dye in PBS (500 nM, S-32703, Invitrogen). Samples were washed with PBS and mounted with ProLong Gold antifade reagent. Some fixed neurons were incubated with 50 μg/ml DNase or RNase (Sigma) for 10 min at room temperature to assess the selectivity of the SYTO labeling.

Image Acquisition and Processing

Images were acquired using an objective EC Plan-Neofluar 40×/1.30 Oil DIC M27 on an Axio-Observer Z1 microscope equipped with AxioCam MRm Rev. 3 (Zeiss, Oberkochen, Germany) and Hamamatsu EM-CCD Imagem (Hamamatsu Photonics, Hamamatsu, Japan) digital cameras. Settings for image acquisition were determined in a random field of a DMSO-treated sample ensuring pixel intensities were within the linear range and avoiding pixel saturation. Images were acquired with ZEN 2 (blue edition) version 2.0.0.0. software (Zeiss). Settings were kept identical for all sampled cells in any given experiment. Whenever possible, five random fields per coverslip and two coverslips per experimental condition were imaged. Most images were acquired with AxioCam, however if cells were imaged in the far red spectrum, the Hamamatsu camera was used.

For figure preparation, the staining of interest (puromycin, calreticulin, SYTO) was converted from grayscale to RGB or to a colorimetric scale (heatmaps) in non-binarized images. Binarized images used for assisted quantification of translation sites were obtained as will be specified below. In all cases

FIGURE 1 | Workflow for puromycin quantification in unprocessed and processed images. **(A)** Workflow A shows puromycin intensity analyses (**path i**) and visual inspection of puromycin translation sites in raw images (**path ii**). After image acquisition, the longest puromycin- and β III-positive neurite (arrowheads in the first panel) was selected with a segmented line, straightened and divided into 10 μm bins with the concentric_circles plugin (**steps 2 and 3**). Mean puromycin intensity per bin, corresponding to protein levels, was measured and represented as the Log₂ (mean puro intensity) vs. distance (**step 4i**). The total fluorescent intensity of the puromycin within the desired interval (soma, neurites, etc. . .) disregarding the bin position is shown as Σ (mean puro intensity; **step 5i**). For visual inspection of puromycin foci, path ii was followed. Number of puromycin foci per bin, corresponding to translation sites, was quantified (Log₂ (# puromycin foci + 1) vs. distance; **step 4ii**). The total number of puromycin foci within the desired interval (soma, neurites, etc. . .) disregarding the bin position is plotted as Σ (# puromycin foci; **step 5ii**). **(B)** The assisted analyses of puromycin-positive foci in binarized images were performed following the workflow B. Once the images were acquired, puromycin staining was filtered with the convolver applying the default normalized kernel and minimum and maximum intensities were adjusted (**steps 1 and 2**). 16-bit images were converted to 8-bit (**step 3**) and binarized with the MaxEntropy mask (**step 4**). Neurites were selected with a segmented line (**step 5**), straightened and binarized with the MaxEntropy mask (**steps 6 and 7**). Discrete puromycin puncta were measured (analyze particles) in neurons in 15 bins covering a distance of 150 μm from the cell nucleus or from the edge of the soma using the concentric_circles plugin (**step 8**). Graphs show the translation sites represented as Log₂ (# puromycin foci + 1) vs. distance (**step 9**). Discrete puromycin foci within desired interval (soma, neurites, etc. . .) disregarding the bin position are represented as Σ (# puromycin foci; **step 10**). Scale bars, 50 μm in whole-cell micrographs and 10 μm in straighten neurites.

background, contrast and sharpness were adjusted and set the same in control and experimental conditions. Markers used as counterstain for neurite selection were adjusted for an optimal visualization in figures.

Puromycin and SYTO Intensity Analysis in Non-binarized Images

To quantify the puromycin fluorescent intensity as a measure of protein production (**Figure 1**; workflow A), the longest puromycin- and β III tubulin-positive neurite or puromycin- and Tau-positive neurite from randomly selected cells was straightened with the Segmented Line tool in FIJI/ImageJ:

FIJI/ImageJ > File > Open (do not autoscale) > Segmented Line (**Figure 1**; workflow A; step 1) > Selection > Straighten (**Figure 1**; workflow A; step 2).

Images obtained from AxioCam measure 1038 \times 1040 pixels, whereas those obtained from the Hamamatsu camera measure 512 \times 512 pixels. Thus, straighten lines were 40 pixel-wide in images taken with the first camera and 20 pixel-wide in images taken with the latter. Since experiments were always compared using a randomized block design (see “Statistical Analyses”), direct comparison between neurites imaged with different cameras is never performed.

Concentric circles at 10 μm intervals emerging from the center of the cell nucleus or from the edge of the soma were generated with an in-house designed FIJI/ImageJ macro (concentric_circles, **Figure 1**; workflow A; step 3) (Quintela-Lopez et al., 2019). 15 bins were generated covering a length of 150 μm of the straighten neurites. Fluorescence intensity was measured in each bin. Background pixel intensity was measured outside the area covered by the neurite and subtracted (**Figure 1**; workflow A; step 4i). To calculate the total fluorescent intensity in the soma, in neurites or in other desired interval disregarding the bin position, values retrieved from each bin of interest were summed up (**Figure 1**; workflow A; step 5i).

The same method was used to measure RNA levels in neurites stained with SYTO.

Note that workflow A (**Figure 1**) exemplifies the procedure in neurites doubly labeled for β II tubulin and puromycin, however it also applies to neurites stained for Tau and puromycin, for SYTO and Tau, for calreticulin and puromycin, etc. . .

Visual Inspection of Puromycin-Positive Translation Foci in Non-binarized Images (Manual Analyses)

As described above, the longest puromycin- and β III-positive neurite, or puromycin- and Tau-positive neurite, etc. . . from randomly selected cells was straightened and divided into 15 10 μm -wide bins with the concentric_circles plugin (**Figure 1**; workflow A; step 3). Discrete puromycin puncta were visually scored in each bin covering a distance of 150 μm from the center of the cell nucleus or from the edge of the soma (**Figure 1**; workflow A; step 4ii). To calculate the total translation foci in the soma or in neurites or in any other desired interval disregarding the bin position, values retrieved from each bin of interest were summed up (**Figure 1**; workflow A; step 5ii). The bin ranging from 0 to 10 μm (first bin within the soma) was discarded as no discrete puncta could be visualized (N/A in **Figures 3D,E**).

Assisted Analyses of Puromycin- and SYTO-Positive Foci in Binarized Images

The assisted analysis of translation sites was performed using the following step-by-step protocol (**Figure 1**; workflow B):

FIJI/ImageJ > File > Open (do not autoscale). Go to the staining of interest (e.g., puromycin) > Process > Filter > Convolve (if a stack is opened, do not process all the images in the stack). The default normalized kernel is sufficient to enhance structures in the periphery of the neurons smaller than 5 \times 5 pixels and it is thus suitable to highlight puromycin-positive translation sites distal to the center of the cell nucleus (**Figure 1**; workflow B; step 1).

Following image convolution:

Image > Adjust > Brightness/Contrast (equal min/max adjustment in all samples within the same experiment; **Figure 1**; workflow B; step 2) > Image > Type > 8-bit (**Figure 1**; workflow B; step 3) > Process > Binary > Make Binary (Method, MaxEntropy; Background, Default; Black background. Only convert current image; **Figure 1**; workflow B; step 4).

Once the image is binarized select the longest positive neurite: Segmented Line (**Figure 1**; workflow B; step 5) > Edit > Selection > Straighten (line width: 20 pixels for Hamamatsu images; 40 pixels for AxioCam images; Process Entire Stack unclicked; **Figure 1**; workflow B; step

6) > Process > Smooth > Process > Binary > Make binary (Method, MaxEntropy; **Figure 1**; workflow B; step 7).

Straighten neurites are finally divided in 15 concentric circles at 10 μm intervals emerging from the center of the cell nucleus or from the edge of the soma with the concentric_circles plugin (**Figure 1**; workflow B; step 8). The number of objects (translation sites...) are scored in each interval (bin) with the Analyze Particles function (default settings; **Figure 1**; workflow B; step 9). To calculate the total translation sites in the soma or in neurites or in any other desired interval disregarding the bin position, values retrieved from each bin of interest were summed up (**Figure 1**; workflow B; step 10).

Although this procedure is described for the puromycin staining as an example, the same steps were followed to binarize and quantify SYTO-positive discrete puncta (RNA) in Tau-positive neurites. When binarization of puromycin and SYTO labeling was performed for the same neurite, colocalization between RNA and protein was performed as follows:

Process > Image Calculator > Image 1 (e.g., puromycin) AND Image 2 (e.g., SYTO; click create new window).

The resulting image is smoothen and binarized with the Mask Entropy mask. The image is finally divided in 15 concentric circles at 10 μm intervals emerging from the edge of the soma with the concentric_circles plugin. The number of objects (considered actively translating RNAs) are scored in each interval (bin) with the Analyze Particles function (default settings).

Intensity Profiles

We used intensity profiles to exemplify fluorescent signal distributions in neurites. Briefly, neurites were selected with the Segmented Line tool (line width: 20 pixels for Hamamatsu images; 40 pixels for AxioCam images) and analyzed with Plot Profile.

Statistical Analyses

The sample size is specified in the figure legends. Statistical analyses were performed with Prism 7 (GraphPad Software, San Diego, CA, United States) following a randomized block design where samples from the same experiment were matched to eliminate inter-experimental variability. When comparing the means of two groups taking one variable into account, two-tailed *t*-tests were performed. When comparing the means of two groups taking two variables into account, two-way ANOVA was used. If more than two groups and more than one variable were analyzed, we performed two-way ANOVA followed by Tukey's multiple comparison test or Holm-Sidak's *post hoc* test depending on the samples requirements.

For correlation analyses we performed a normality test on the data to determine if they followed a Gaussian distribution, which most of them didn't. Thus, we chose to perform Spearman non-parametric correlation test to retrieve the correlation coefficients. In the correlation graphs, linear regression of the data was performed to evaluate the differences between slopes (ANCOVA).

Note that in some cases, Y axes are represented as Log2 of the actual measured raw values to better visualize the results. In

other experiments where some values equaled zero, one unit was added to all values in order to apply a Log2 function. Regardless of the transformation, all statistical analyses were performed on raw data and not on transformed data.

RESULTS

Detection of Newly Synthesized Neuritic Proteins by Puromycilation

Based on previously published data (Baleriola et al., 2014), rat hippocampal neurons grown for 9 days *in vitro* (DIV) were treated with vehicle (DMSO) or 3 μM $\text{A}\beta_{1-42}$ oligomers for 24 h by bath application. As a first step to quantify RNA translation sites in neurites we first detected *de novo* production of neuritic proteins by puromycilation/SUnSET (Schmidt et al., 2009; **Figure 2A**). The antibiotic puromycin is an aminoacyl-tRNA analog that incorporates into the polypeptide chains during translation elongation, leading to translation termination (Yarmolinsky and Haba, 1959). The development of specific antibodies has allowed the immunodetection of puromycilated polypeptides as a measure of protein synthesis. Control and $\text{A}\beta$ -treated cells were fed with 2 μM puromycin for 30 min prior to fixation. Following fixation with a PFA/sucrose mix, cells were stained for puromycin and counterstained with an anti- β III tubulin antibody to visualize the neuronal cytoskeleton (**Figure 2A**). As a negative control, immunostaining was performed on neurons that had not been treated with puromycin (-puro, **Figure 2A**). Fluorescence intensity for the raw puromycin signal, represented in a colorimetric scale (**Figure 2A**), was measured along the longest puromycin- and β III-positive neurite in randomly selected cells (1–6, **Figure 2A**). Fluorescence levels in puromycin-labeled neurites (3 and 4, **Figures 2A–C**) were well above the levels measured in negative controls (1 and 2, **Figures 2A–C**). Additionally, puromycin hotspots were readily visible in distal sites of the neurites, especially in $\text{A}\beta$ -treated cells (4, intensity profile and heatmap in **Figure 2B**). Finally, regardless of the effect of $\text{A}\beta_{1-42}$, puromycin intensity was significantly reduced in neurites when cells were co-incubated with the translation inhibitor anisomycin (+ anis + puro, **Figure 2A**; 5 and 6, **Figures 2A–C**). Altogether these results indicate that in our system puromycin labeling can be used to detect *de novo* synthesis of neuritic proteins as previously reported in similar experimental setups (Walker et al., 2018; Rangaraju et al., 2019).

$\text{A}\beta_{1-42}$ Oligomers Increases New Synthesis of Neuritic Proteins Detected Beyond the Canonical Endoplasmic Reticulum

Then we asked whether the puromycin signal likely arose from the endoplasmic reticulum (ER). Soma-centric views consider that most protein synthesis in eukaryotic cells occurs in the ER (specifically in the rough ER). In neurons, however, the positioning of the rough ER (RER) with respect to distal sites of neurites does not explain how in some experimental

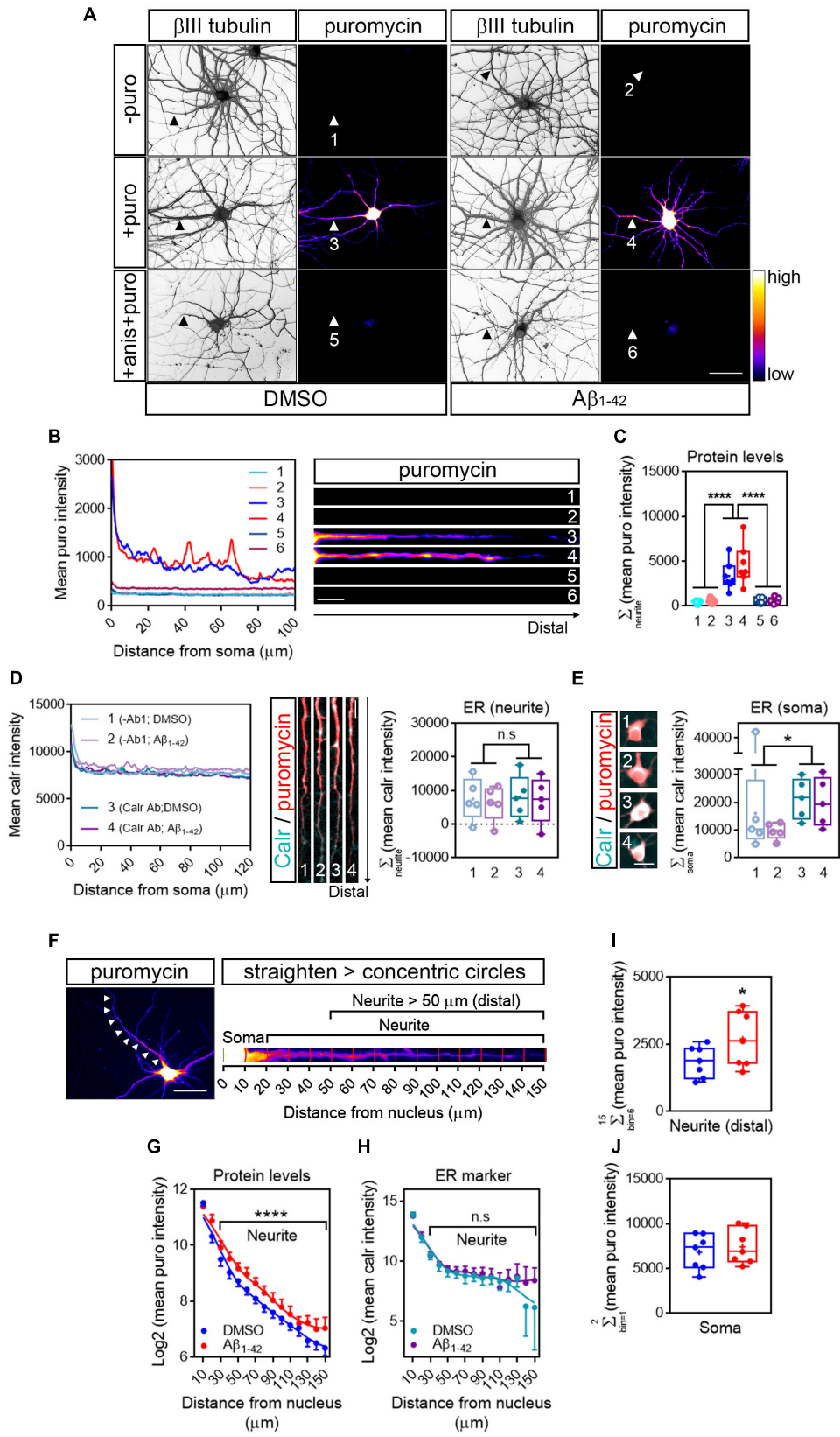


FIGURE 2 | Continued

FIGURE 2 | Detection of newly synthesized proteins by puromycylation. **(A)** Rat hippocampal neurons were grown for 9 DIV and were treated with DMSO (left panels) or A β_{1-42} oligomers (right panels) for 24 h. Before fixing, cells were incubated with vehicle (-puro; neurites 1 and 2), with puromycin (+ puro; neurites 3 and 4) or with puromycin and anisomycin (+ anis + puro; neurites 5 and 6) for 30 mins. Cells were immunostained with an anti- β III tubulin antibody to visualize the neuronal cytoskeleton (gray) and with an anti-puromycin antibody to analyze newly synthesized proteins (heatmaps). Scale bar, 50 μ m. **(B)** Intensity profiles were measured in the longest puromycin- and β III tubulin-positive neurite from randomly selected cells as exemplified. 1 and 2: no puromycin incubation in DMSO- and A β -treated neurons, respectively. 3 and 4: 30 min puromycin incubation in DMSO- and A β -treated cells, respectively. 5 and 6: co-incubation with anisomycin and puromycin for 30 mins in DMSO- and A β -treated cells, respectively. Scale bar, 10 μ m in heatmaps. **(C)** Box and whisker graph representing protein levels as the total fluorescent intensity of the puromycin staining along 130 μ m of β III tubulin-positive neurites. 1 and 2: no puromycin incubation in DMSO- and A β -treated neurons, respectively. 3 and 4: 30 min puromycin incubation in DMSO- and A β -treated cells, respectively. 5 and 6: co-incubation with anisomycin and puromycin for 30 mins in DMSO- and A β -treated cells, respectively. Data represent the average value of 5–10 sampled cells per condition shown as individual data points, and the mean and median of 7 independent experiments ($n = 7$). **** $p < 0.0001$; two-way ANOVA followed by Tukey's multiple comparison test. **(D)** The "canonical" endoplasmic reticulum (ER) was defined by Calreticulin staining (Calr Ab in intensity profiles). To determine the background signal, some cells were stained only with the secondary antibody (no-primary antibody control; -Ab1 in intensity profiles). Images exemplify neurites processed for calreticulin staining (cyan) to measure the area covered by the ER and counterstained with an anti-puromycin antibody (red). Box and whisker graph representing the total fluorescent intensity of the calreticulin staining along 130 μ m of calreticulin- and puromycin-positive neurites. 1 and 2: no-primary antibody control (-Ab1) in DMSO- and A β -treated neurons, respectively. 3 and 4: calreticulin antibody incubation (Calr Ab) in DMSO- and A β -treated neurons, respectively. Data represent the average value of 5–10 sampled cells per condition shown as individual data points, and the mean and median of 5 independent experiments ($n = 5$). n.s., no significant; two-way ANOVA followed by Holm-Sidak's *post hoc* test. Scale bar, 10 μ m. **(E)** Calreticulin immunostaining signal (cyan) in somata from DMSO- and A β -treated cells and counterstained with an anti-puromycin antibody (red). Scale bar, 10 μ m in images. Box and whisker graph representing the total fluorescent intensity of the calreticulin staining along the first 20 μ m of calreticulin- and puromycin-positive somata. 1 and 2: no-primary antibody control (-Ab1) in DMSO- and A β -treated neurons, respectively. 3 and 4: calreticulin antibody incubation (Calr Ab) in DMSO- and A β -treated neurons, respectively. Data represent the average value of 5–10 sampled cells per condition shown as individual data points, and the mean and median of 5 independent experiments ($n = 5$). * $p < 0.05$; two-way ANOVA followed by Holm-Sidak's *post hoc* test. Scale bar, 20 μ m. **(F)** Cells were processed for puromycin staining to measure protein synthesis (heatmap) and counterstained with an anti- β III tubulin antibody to visualize the neuronal cytoskeleton (not shown). The longest positive neurite (arrowheads in left micrograph) was selected with a segmented line, straighten and divided into 10 μ m bins with the concentric_circles plugin (straighten neurite right) following workflow Ai in **Figure 1**. Scale bar, 50 μ m. **(G)** Puromycin intensity was measured in DMSO- and A β -treated neurons in 15 bins covering a distance of 150 μ m from the cell nucleus (as also shown in the straighten micrograph exemplified in **(F)**). The graph shows the average intensity of puromycin per condition represented as Log₂ (mean puro intensity) vs. distance \pm SEM measured in 7 independent experiments ($n = 7$). **** $p < 0.0001$; two-way ANOVA. **(H)** Calreticulin intensity was measured in DMSO- and A β -treated neurons in 15 bins covering a distance of 150 μ m from the cell nucleus. The graph shows the average intensity of calreticulin per condition represented as Log₂ (mean calr intensity) vs. distance \pm SEM measured in 5 independent experiments ($n = 5$). n.s., no significant; two-way ANOVA. **(I)** Box and whisker graphs representing the total fluorescent intensity of the puromycin staining in β III tubulin- and puromycin-positive neurites within the range of 50–150 μ m from the nucleus [Neurite (distal)] as also exemplified in **(F)**. Data represent the average value of 5–10 sampled cells per condition shown as individual data points, and the mean and median of 7 independent experiments ($n = 7$). * $p < 0.05$; two-tailed *t*-test. **(J)** Box and whisker graphs representing the total fluorescent intensity of the puromycin staining in β III tubulin- and puromycin-positive somata within the range of 0–20 μ m from the nucleus (Soma) as also exemplified in **(F)**. Data represent the average value of 5–10 sampled cells per condition shown as individual data points, and the mean and median of 7 independent experiments ($n = 7$).

setups that allow to study the local response of dendrites and axons (reviewed in Holt et al., 2019) newly synthesized proteins are detected peripherally, unless they are produced locally beyond the "canonical" ER. The RER is enriched in proteins involved in the folding of nascent polypeptides, being the Calnexin/Calreticulin system one the best known protein complexes (Rutkevich and Williams, 2011). After culturing hippocampal neurons for 9 days and following 24-h treatments with DMSO or A β_{1-42} , neurons were labeled with puromycin. Cells were then processed for Calreticulin (Calr) and puromycin immunostaining. As a negative control, some neurons were subjected to the immunocytochemistry procedure but were not incubated with anti-Calr antibody (no-primary antibody control). To determine the presence of Calreticulin in neurites we compared the fluorescent signal of cells incubated with anti-Calr antibody with those incubated with no primary antibody (**Figure 2D**). Results showed that both DMSO- and A β -treated neurites were devoid of Calreticulin, and thus of "canonical" ER (**Figure 2D**, right graph). Conversely, Calreticulin could be detected above background levels in neuronal somata of cells treated with DMSO or A β_{1-42} oligomers (**Figure 2E**).

We then asked whether A β oligomers induced changes in the distribution pattern of newly synthesized proteins along neurites, beyond the canonical ER domain. The longest

puromycin-positive neurite (**Figure 2F**; left micrograph) of randomly selected cells was straighten and divided into 10 μ m bins following the workflow Ai (**Figure 1**). Puromycin intensity was measured in 15 bins covering a length of 150 μ m from the center of the cell nucleus using the concentric_circles plugin in Fiji/ImageJ (**Figure 2F**; right micrograph). A significantly distinct distribution in the levels of newly produced proteins was observed in A β -treated neurites compared to controls (positions beyond 20 μ m, **Figure 2G**). In line with the absence of a canonical ER in neurites, no differences were detected in the Calreticulin staining pattern between DMSO- and A β -treated neurites (**Figure 2H**). Finally, we focused on neuritic positions distal to the ER to increase the chances that newly synthesized proteins measured in neurites did not rely on the ER-dependent translation machinery. We summed up puromycin intensity signals in bins corresponding to the 50 to 150 μ m range measured from the center of the nucleus (distal neurite; **Figure 2I**). A β_{1-42} significantly increased the levels of newly synthesized proteins in this interval. More importantly the effect of A β was restricted to neurites and did not affect the neuronal soma (**Figure 2J**) in accordance with previously published data (Walker et al., 2018).

It is noteworthy pointing out that in our experimental system the effect of A β oligomers was not evident with puromycin pulses shorter than 30 min (e.g., 10 min. Data not shown).

Image Processing Unravels a Previously Unreported Effect of A β _{1–42} Oligomers on Translation Foci in Neurites

Measuring puromycin intensity can give an idea of the amount of protein being produced distal from the ER within neurites and/or diffused from the actual translation site, but it does not report on the number and position of the translation sites themselves. In the case of A β treated cells, increased puromycin intensity might be a result of the emergence of new translation sites, a consequence of an increased rate of protein production in preexisting sites or both. To determine whether A β oligomers modify the amount of translation sites in neurites we quantified the number of puromycin discrete puncta. Discrete puncta in distal neuritic sites likely reflect foci of localized translation (Graber et al., 2013; Rangaraju et al., 2019). Such foci can be easily overlooked since their intensity can be ~20 to 30 times less than somatic puromycin fluorescent levels (as implicitly shown in **Figure 2**). We have developed a strategy to enhance puromycin hotspots in neurites based solely on image processing and the assisted quantification of the resulting objects (**Figure 1**; workflow B).

The number of discrete puromycin foci was quantified along the longest puromycin- and β III tubulin-positive neurite of randomly sampled cells (**Figure 3A**). Image acquisition was identical in control and A β -treated neurons. We selected neurites from raw and binarized images in order to compare quantifications performed by visual inspection of the puromycin staining (manual; **Figures 1, 3**, workflow A) and by analyzing particles (assisted; **Figures 1, 3**, workflow B), respectively. On the one hand DMSO- and A β -treated neurites were selected from raw images (represented as heatmaps; 1 and 2 in **Figure 3A**) with a segmented line 20 or 40 pixels wide and straighten (1 and 2; **Figure 3B**). On the other hand, images were filtered with the convolver in FIJI/ImageJ applying the default normalized kernel. The default kernel was sufficient to enhance structures in the periphery of the neurons and thus was suitable to highlight puromycin-positive translation foci distal to the center of the cell nucleus. Published data have reported spot quantification procedures without applying convolution filters. However, in our case image filtering prior to binarization enhanced the detection of discrete foci compared to unfiltered images, especially in A β -treated neurons (condition 2 in **Supplementary Figure S1**).

Following image convolution, minimum and maximum intensities (B&C menu in FIJI/ImageJ) were then manually adjusted in order to eliminate pixels outside the stained cells (background) and enhance the intensity of those inside. 16-bit images were converted to 8-bit and binarization was performed using the MaxEntropy mask. As in the case of the raw images, DMSO- and A β -treated neurites were selected with a 20- or 40-pixel wide segmented line and straighten. Finally, straighten neurites were smoothen and binarized again using the MaxEntropy mask (1 and 2; **Figure 3C**). As exemplified by the number of peaks in the intensity profiles image conversion increased the number of detected sites (foci in **3B** and **C**) and slightly enhanced the effect of A β oligomers, which increased from 2.7- to 3.3-fold. We then analyzed the distribution pattern of translation foci along neurites. Neurites were divided into

10 μ m bins and positive puromycin puncta within each bin were visually scored prior to image conversion (1 and 2 in **Figure 3D**; wA) or were counted with the particle analyzer in binarized images (1 and 2 in **Figure 3D**; wB). In all cases 15 bins were quantified per cell, covering a distance of 150 μ m from the cell nucleus. Both quantification methods revealed a significantly distinct distribution of translation sites in neurites in A β -treated cells compared to controls (**Figure 3E**). However, an average of almost 10-fold increase in the number of total foci in neurites was observed when using the assisted quantification method compared to visual inspection (**Figures 3E,F**).

The default matrix in FIJI's convolver is a Laplacian operator-based edge detector that allows to find discontinuities in the puromycin labeling that could result from a punctate staining arising from discrete positive foci. Laplacian operators are very accurate in finding edges in an image but also very sensitive to background noise. Thus, we quantified the amount of foci also in neurons that had not been fed with puromycin. Negative controls showed significantly less amount of foci in neurites regardless of whether quantification was performed manually in non-binarized images (**Figure 3F**; left graph) or with the particle analyzer in filtered and binarized images (**Figure 3F**; right graph). In conclusion the 5 \times 5 Laplacian operator used in our approach can be successfully applied to highlight positive translation foci in distal neuritic sites.

When comparing the scores performed at each distance by manual inspection in raw images and with the assisted method in binarized images we observed a significant positive correlation between both procedures that ranged from moderate to high in DMSO- and A β -treated cells, respectively (**Figure 3G**). To determine which method was closer to the unbiased measurement of protein production represented by puromycin intensity (**Figure 2**), we then compared data obtained from binarized images and from raw images with the intensity values. In both cases we found a significant high positive correlation (**Figure 3H**). However, when fitting the translation sites at each distance to a regression line, a significant increase in the slope was observed when data were obtained from binarized images, suggesting increased similarities between the number of discrete puromycin foci and puromycin intensity values when using the assisted quantification method.

Finally, we focused on distal sites of the neurites (> 50 μ m from the nucleus) disregarding the bin position and were unable to detect any significant change between DMSO- or A β -treated cells when translation foci were quantified in raw images by visual inspection (manual, **Figure 3I**; wA). Conversely, we did observe a significant effect of A β oligomers when quantification was performed with the particle analyzer in binarized images (assisted, **Figure 3I**; wB). In no case did we detect any changes induced by A β in the soma (**Figure 3I**). Altogether, results so far indicate that binarizing images from puromycin-positive cells allows the assisted quantification of neuritic translation sites yielding results that resemble those obtained from an unbiased measurement of raw puromycin intensity. Additionally, assisted quantification in binarized

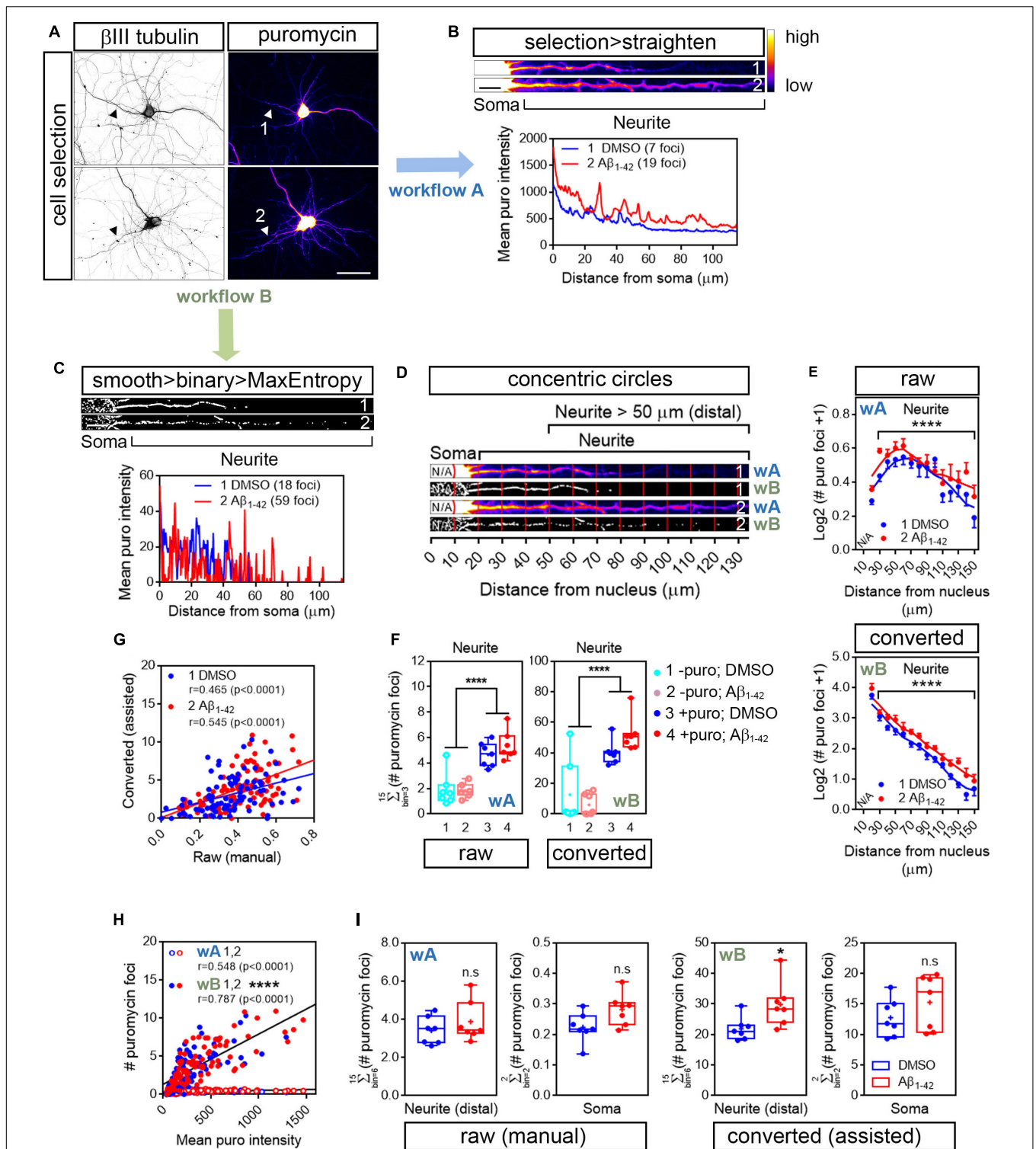


FIGURE 3 | Image processing reveals an effect of $A\beta_{1-42}$ oligomers on neuritic translation sites. **(A)** Rat hippocampal neurons were grown for 9 DIV and were treated with DMSO or $A\beta_{1-42}$ oligomers for 24 h. Cells were incubated with puromycin for 30 mins and processed for β III tubulin (gray) and puromycin immunostaining (heatmaps). Scale bar, 50 μ m. **(B)** Following workflow A, the longest puromycin- and β III-positive neurite in raw images was selected with a segmented line and straighten. Puromycin-positive discrete puncta were analyzed by visual inspection as exemplified in the intensity profiles obtained from straighten neurites (heatmaps). 1 and 2: 30 min puromycin incubation in DMSO- and $A\beta$ -treated cells, respectively. Scale bar, 10 μ m. **(C)** Following workflow B, selected neurites were straighten, smoothen and binarized with the MaxEntropy mask (smooth > binary > MaxEntropy). Puromycin-positive discrete puncta were analyzed (Continued)

FIGURE 3 | with the particle analyzer as exemplified in the intensity profiles from straighten neurites. 1 and 2: 30 min puromycin incubation in DMSO- and A β -treated cells, respectively. Scale bar, 10 μ m. **(D)** Discrete puromycin puncta were measured in DMSO- and A β -treated neurons in 15 bins covering a distance of 150 μ m from the cell nucleus using the concentric_circles plugin. Measurements were performed by visual inspection in raw images (workflow Aii, wA) and with the particle analyzer in binarized images (workflow B, wB). 1: DMSO-; 2: A β -treated neurites. N/A, not applicable. **(E)** Graphs show the average puromycin foci per condition represented as Log2 (# puro foci + 1) vs. distance \pm SEM measured in raw (wA) and binarized images (wB) from 7 independent experiments ($n = 7$). **** $p < 0.0001$; two-way ANOVA. N/A, not applicable. **(F)** Box and whisker graph representing translation sites as the total number of puromycin foci along 130 μ m of β III tubulin-positive neurites following visual inspection of raw images (raw; workflow A, wA) or assisted quantification in binarized images (converted; workflow B, wB). 1 and 2: no puromycin incubation in DMSO- and A β -treated neurons, respectively. 3 and 4: 30 min puromycin incubation in DMSO- and A β -treated cells, respectively. Data represent the average value of 5–10 sampled cells per condition shown as individual data points, and the mean and median of 7 independent experiments ($n = 7$). **** $p < 0.0001$; two-way ANOVA followed by Holm-Sidak's *post hoc* test. **(G)** Spearman correlation between quantifications in raw and in binarized images. Graphs represent each scored value per distance using both methods in DMSO- (1, blue) and A β -treated neurons (2, red) cultured in 7 independent experiments ($n = 7$). $p < 0.05$ indicate a significant correlation. **(H)** Spearman correlation between non-assisted (wA; 1, DMSO-; 2, A β -treated cells) or assisted quantification (wB; 1, DMSO-; 2, A β -treated neurons) of translation sites (# puromycin foci) and protein production (mean puro intensity). Graphs represent each scored value per distance from 7 independent experiments ($n = 7$). $p < 0.05$ indicate a significant correlation. **** $p < 0.0001$; significant differences between slopes. **(I)** Box and whisker graphs representing the total puromycin foci in β III tubulin- and puromycin-positive neurites within the range of 50 to 150 μ m [Neurite (distal)] and in the soma (soma; 10–20 μ m) following visual inspection of raw images (raw (manual); workflow A, wA) or assisted quantification in binarized images (converted (assisted); workflow B, wB). Data represent the average value of 5–10 sampled cells per condition shown as individual data points, and the mean and median of 7 independent experiments ($n = 7$). * $p < 0.05$; n.s., no significant; two-tailed *t*-test.

images enhances the effect of A β_{1-42} oligomers on discrete puromycin puncta in distal neurites.

Image Processing Reveals an Increase in Translation Foci in Axons in Response to A β_{1-42} Oligomers

The first evidence of A β oligomers regulating local translation in neurons was reported in axons (Baleriola et al., 2014). Thus, we next tried our assisted quantification method in neurites positive for the axonal protein Tau. Additionally, after treatment with DMSO or A β oligomers for 24 h, we fed the cells with puromycin for 5, 10, or 30 min. Shorter puromycin pulses were tested to decrease the chances of protein diffusion from the actual translation site. We additionally sought to test whether the rate of puromycin incorporation in axons, unlike in all β III tubulin-positive neurites, allowed us to detect increased translation in response to A β oligomers with pulses as short as 5 min. 5- and 10-min puromycin treatments have been successfully used to detect localized translation in neurites in other experimental setups (Graber et al., 2013; Walker et al., 2018; Rangaraju et al., 2019).

We first analyzed the distribution pattern of puromycin intensity along Tau-positive neurites. The longest puromycin-, Tau-positive neurite was selected from randomly sampled cells imaged with identical settings. Neurites from raw images (exemplified as heatmaps in **Figure 4A**) were straighten and divided into 10 μ m bins. Puromycin intensity was measured in 15 bins covering a distance of 150 μ m from the edge of the soma (**Figure 4B**). No changes in newly synthesized proteins were observed between control and A β -treated cells when neurons were exposed to puromycin for 5 or 10 min. However, a significantly distinct pattern in protein production induced by A β oligomers was detected in Tau-positive neurites following a 30-min treatment with puromycin (**Figure 4B**). Focusing on distal sites of the neurite (beyond 30 μ m from the soma in these sets of experiments) we observed a significant accumulation of newly synthesized proteins after 30 min of puromycin treatment compared to shorter exposures in both DMSO- and A β -treated cells. A significant increase in puromycin

intensity in A β -treated neurites compared to controls was also detected with the longest puromycin exposure (**Figure 4C**). These results, similar to the ones obtained in β III tubulin-positive neurites, confirm that A β_{1-42} oligomers induce *de novo* synthesis of axonal proteins as previously reported (Baleriola et al., 2014; Walker et al., 2018). We then quantified the number of discrete puromycin foci in binarized images. Images were convolved with the default normalized kernel in FIJI/ImageJ and processed like β III tubulin neurites as described before (**Figure 4D**). Translation foci were scored with the particle analyzer in 15 bins covering a distance of 150 μ m from the edge of the cell body. Again, a distinct pattern of translation was observed between DMSO- and A β -treated neurites only when cells were fed with puromycin for 30 min (**Figure 4E**). Similarly, despite detecting a significant accumulation of discrete puromycin foci in both control and A β -treated cells after 30 min of puromycin exposure compared to shorter pulses, these were significantly higher when A β oligomers were added to the cultures (**Figure 4F**).

To determine if our assisted scoring method correlated better than manual quantification with the unbiased measurements of fluorescence intensity also in Tau-positive neurites, two independent observers quantified the number of puromycin-positive puncta along neurites by visual inspection of raw images (**Figures 4G–J**). Both observers reported a significantly distinct distribution of discrete foci in DMSO- and A β -treated samples when scores were performed in 10 μ m bins (**Figures 4G,I**). However, when focusing on distal sites of the neurites (> 30 μ m from the soma) disregarding the bin position, none of them detected changes between controls and A β treatments (**Figures 4H,J**), in line with previous results (**Figure 3I**). Data retrieved from observer 1 revealed a low yet significant correlation between scores obtained in binarized images and those obtained in raw images in both control and A β -treated neurons, whereas the correlation between both scoring methods was only significant upon A β treatment based on results from observer 2 (**Figure 4K**). We then compared data obtained from binarized images and the averaged data retrieved from observers 1 and 2 with the intensity values. We found no significant correlation between the fluorescent intensity at each

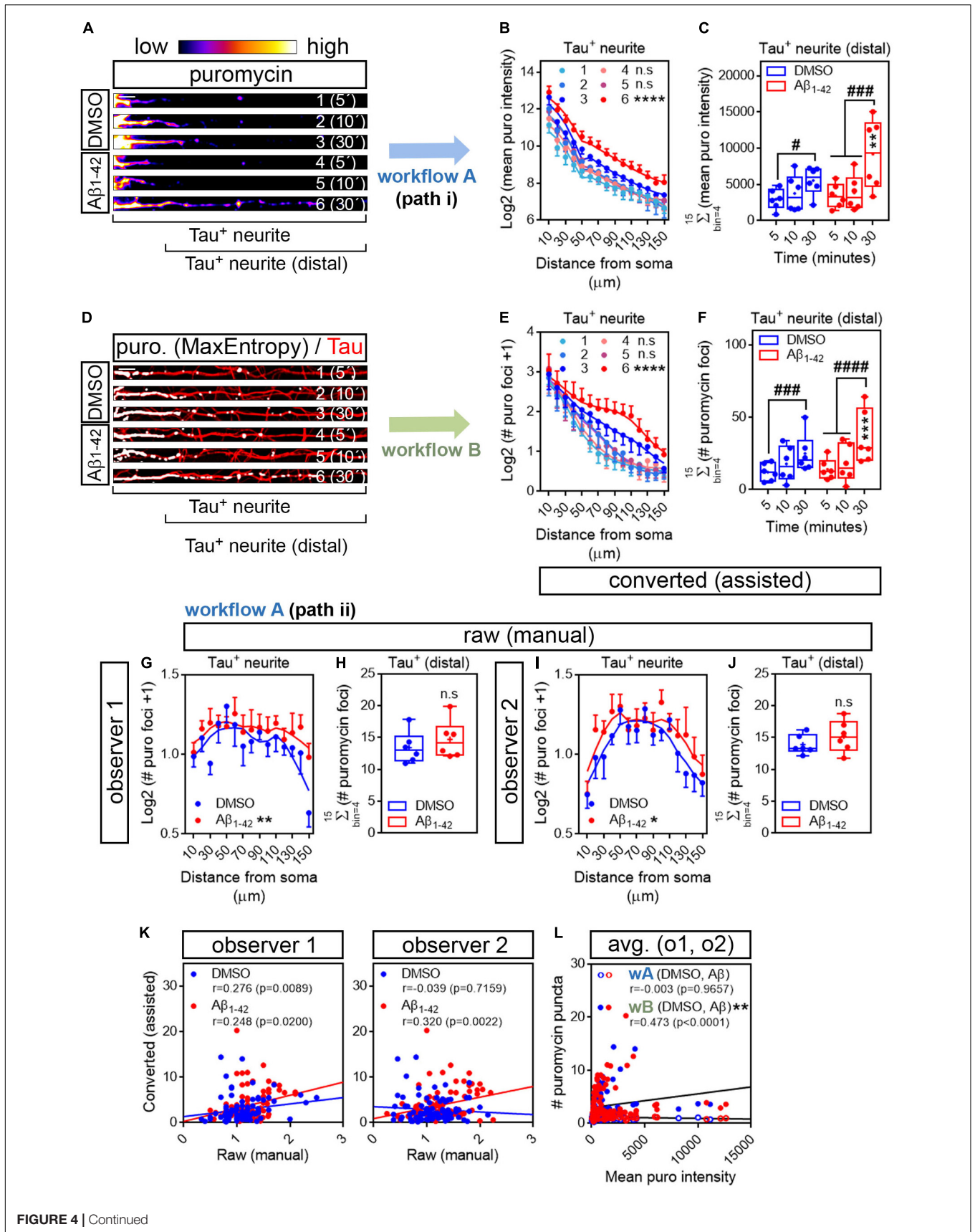


FIGURE 4 | Continued

FIGURE 4 | $A\beta_{1-42}$ oligomers increase translation sites in Tau-positive neurites. **(A)** Rat hippocampal neurons were grown for 9 DIV and treated with DMSO or with $A\beta_{1-42}$ oligomers for 24 h. Cells were fed with puromycin for 5, 10 or 30 mins, fixed and immunostained with an anti-puromycin antibody to measure protein synthesis (heatmaps) and counterstained with an anti-Tau antibody (not shown). The longest Tau- and puromycin-positive neurite was selected with a segmented line and straightened. 1, 2, and 3, DMSO-treated cells exposed to puromycin for 5, 10, and 30 mins, respectively; 4, 5 and 6, $A\beta$ -treated cells exposed to puromycin for 5, 10, and 30 mins, respectively. Scale bar, 10 μm . **(B)** Puromycin intensity was measured in DMSO- and $A\beta$ -treated neurons in 15 bins covering a distance of 150 μm from the edge of the soma (Tau⁺ neurite) following workflow Ai in raw images. The graph shows the average intensity of puromycin per condition represented as Log₂ (mean puromycin intensity) vs. distance \pm SEM measured in 6 independent experiments ($n = 6$). 1, 2, and 3, DMSO-treated cells exposed to puromycin for 5, 10, and 30 mins respectively; 4, 5, and 6, $A\beta$ -treated cells exposed to puromycin for 5, 10, and 30 mins, respectively. **** $p < 0.0001$, DMSO vs. $A\beta$, 30 mins puromycin; two-way ANOVA followed by Tukey's multiple comparison test. **(C)** Box and whisker graphs representing the total fluorescent intensity of the puromycin staining in Tau-positive neurites within the range of 30 to 150 μm [Tau⁺ neurite (distal) as exemplified in **(A)**]. Data represent the average value of 10–20 sampled cells per condition shown as individual data points, and the mean and median of 6 independent experiments ($n = 6$). # $p < 0.05$ 5 vs. 30 mins puromycin in DMSO-treated cells; ### $p < 0.001$ 5 vs. 30 mins and 10 vs. 30 mins in $A\beta$ -treated neurons; ** $p < 0.01$ DMSO vs. $A\beta$, 30 mins puromycin; two-way ANOVA followed by Tukey's multiple comparison test. **(D)** The longest puromycin- and Tau-positive neurite was selected with a segmented line and straightened, smoothed and binarized with the MaxEntropy mask (MaxEntropy). Counterstain with the anti-Tau antibody is shown (red). 1, 2, and 3, DMSO-treated cells exposed to puromycin for 5, 10, and 30 mins, respectively; 4, 5 and 6, $A\beta$ -treated cells exposed to puromycin for 5, 10, and 30 mins, respectively. Scale bar, 10 μm . **(E)** Puromycin-positive discrete foci were scored with the particle analyzer in 15 bins covering a distance of 150 μm from the edge of the soma (Tau⁺ neurite) as explained in workflow B. The graph shows the average translation events per condition represented as Log₂ (# puromycin foci + 1) vs. distance \pm SEM measured in 6 independent experiments ($n = 6$). 1, 2, and 3, DMSO-treated cells exposed to puromycin for 5, 10, and 30 mins, respectively; 4, 5 and 6, $A\beta$ -treated cells exposed to puromycin for 5, 10, and 30 mins, respectively. **** $p < 0.0001$ DMSO vs. $A\beta$, 30 mins puromycin; two-way ANOVA followed by Tukey's multiple comparison test. **(F)** Box and whisker graphs representing the total number of translation events scored in Tau-positive neurites within the range of 30 to 150 μm (Tau⁺ neurite (distal) as exemplified in **(D)**). Data represent the average value of 10–20 sampled cells per condition shown as individual data points, and the mean and median of 6 independent experiments ($n = 6$). ### $p < 0.001$ 5 vs. 30 mins puromycin in DMSO-treated cells; #### $p < 0.0001$ 5 vs. 30 mins and 10 vs. 30 mins in $A\beta$ -treated neurons; *** $p < 0.001$ DMSO vs. $A\beta$, 30 mins puromycin; two-way ANOVA followed by Tukey's multiple comparison test. **(G)** Discrete puromycin puncta scored by observer 1 in DMSO- and $A\beta$ -treated neurons in 15 bins covering a distance of 150 μm from the edge of the soma (Tau⁺ neurite) and in **(H)** distal sites of Tau-positive neurites disregarding the bin position [Tau⁺ (distal)]. **(I)** Discrete puromycin puncta scored by observer 2 in DMSO- and $A\beta$ -treated neurons in 15 bins covering a distance of 150 μm from the edge of the soma (Tau⁺ neurite) and in **(J)** distal sites of Tau-positive neurites disregarding the bin position [Tau⁺ (distal)]. All measurements were performed by visual inspection in raw images according to workflow Aii. Graphs in **(G)** and **(I)** show the average number of translation events per condition represented as Log₂ (# puromycin foci + 1) vs. distance \pm SEM measured following a 30-min puromycin pulse in 6 independent experiments ($n = 6$). * $p < 0.05$; ** $p < 0.01$; two-way ANOVA followed by Tukey's multiple comparison test. Box and whisker graphs in **(H,J)** show the total number of translation events scored in Tau-positive neurites within the range of 30 to 150 μm [Tau⁺ (distal)]. Data represent the average value of 10–20 sampled cells per condition shown as individual data points, and the mean and median of 6 independent experiments ($n = 6$). n.s., no significant; two-tailed *t*-tests. **(K)** Spearman correlation between quantifications in raw (manual) and in binarized (assisted) images. Graphs show values scored in raw (manual) images by observer 1 and observer 2 in DMSO- (blue) and $A\beta$ -treated neurons (red) cultured in 6 independent experiments ($n = 6$). $p < 0.05$ indicate a significant correlation. **(L)** Spearman correlation between non-assisted [wA (DMSO, $A\beta$)] or assisted quantification [wB (DMSO, $A\beta$)] of translation sites (# puromycin foci) and protein production (mean puromycin intensity). Graphs represent the non-assisted counts per distance as the average score obtained by observers 1 and 2. Data correspond to 6 independent experiments ($n = 6$). $p < 0.05$ indicate a significant correlation. ** $p < 0.01$; significant differences between slopes.

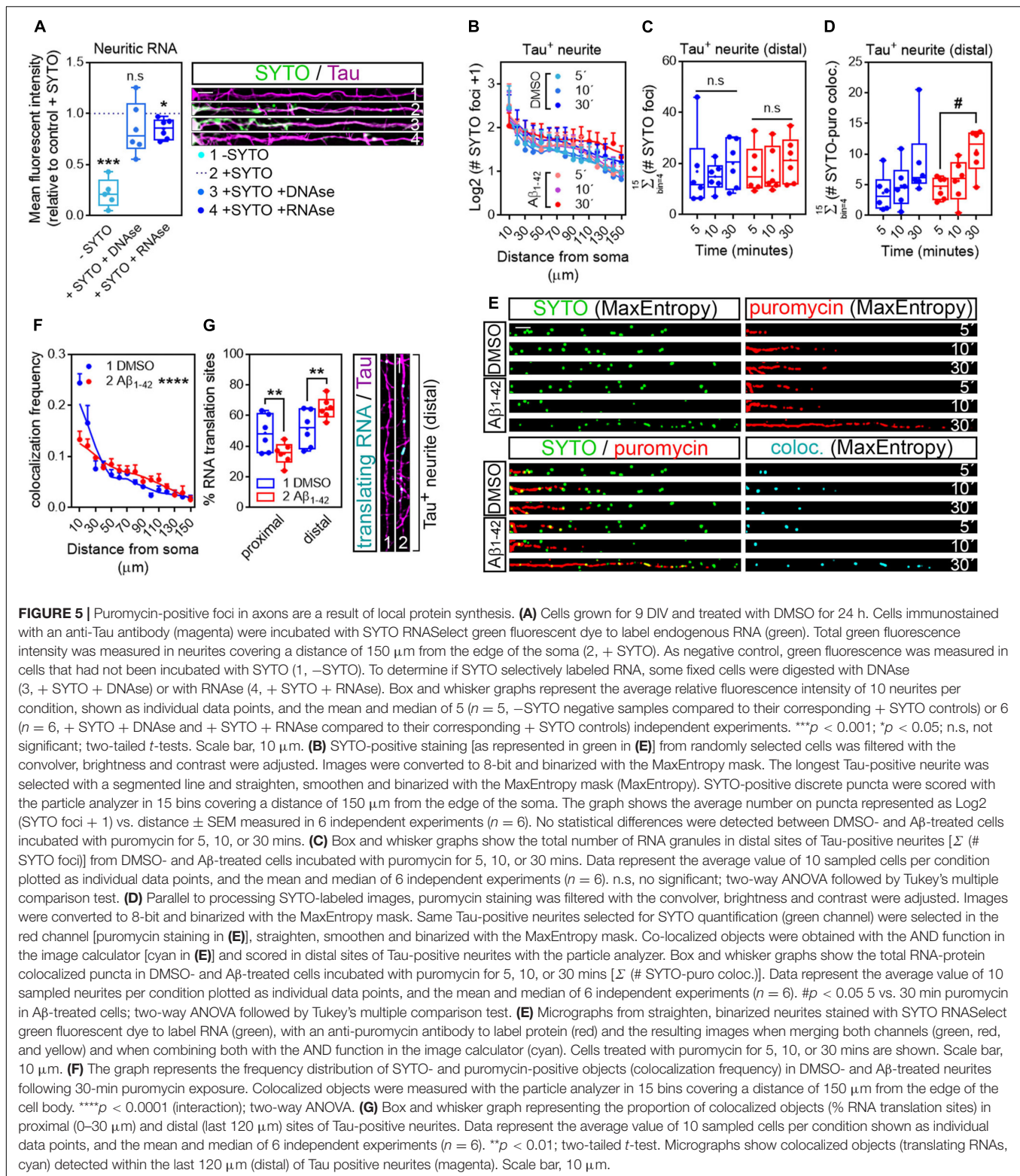
neuritic position and the number puromycin foci scored by visual inspection (wA, **Figure 4L**). Conversely, a significant moderate positive correlation was observed between parameters when translation sites were counted in binarized images with the particle analyzer (wB, **Figure 4L**). Furthermore, when fitting the translation sites at each distance to a regression line, a significant increase in the slope was observed when data were obtained from binarized images, suggesting increased similarities between the number of puromycin foci and the puromycin intensity when using the assisted quantification method (**Figure 4L**). These results not only confirm that scoring puromycin-positive sites in neurites in binarized images by assisted means show a better fit with the unbiased measurement of raw puromycin intensity, but also reveal an effect of $A\beta$ oligomers on discrete translation sites in neurites that was previously unreported.

Object-Based Colocalization Analyses Confirm That Peripheral Translation Sites in Axons Arise From Localized RNAs

As mentioned previously, discrete puromycin-positive puncta in distal neurites likely reflect sites of local translation. Nevertheless, we sought to determine if in our system what we had reported as neuritic translation sites did in fact colocalize with neuritic

RNAs. Samples processed for puromycin detection in Tau-positive neurites were incubated for 20 min with 500 nM SYTO RNaselect, a fluorescent dye that selectively binds RNA (Savas et al., 2010). To verify that SYTO could be successfully used in our system to label neuritic RNA we compared the fluorescent intensity of the dye within Tau-positive neurites to background fluorescent levels in cells that had not been incubated with SYTO. Additionally, some fixed cells were digested with 50 $\mu\text{g}/\text{ml}$ DNase or RNase prior to labeling. Neurites from SYTO-positive cells showed significantly higher levels of fluorescence than those not incubated with the dye (Compare dashed line with -SYTO in graph and neurites 1 and 2 in **Figure 5A**). More importantly, levels of SYTO were similar in positive neurites incubated in the presence or absence of DNase (Compare dashed line with + SYTO + DNase in graph and neurites 2 and 3 in **Figure 5A**), whereas incubation with RNase moderately yet significantly reduced the fluorescence intensity (Compare dashed line with + SYTO + RNase in graph and neurites 2 and 4 in **Figure 5A**). These results indicate that indeed neuritic RNAs can be labeled with SYTO RNaselect dye.

We then analyzed the distribution of RNA granules, measured as SYTO-stained foci, along Tau-positive neurites. For this purpose, raw images stained for SYTO were processed following the exact same protocol as for puromycin labeling (**Figure 1**;



workflow B): images were convolved with the default normalized kernel in Fiji/ImageJ, minimum and maximum intensity values were adjusted, 16-bit images were converted to 8-bit and binarized using the MaxEntropy mask. Neurites were

then selected with a segmented line, straighten, smoothen and binarized again with the MaxEntropy function (green, Figure 5E). The number of RNA granules was scored in 15 bins covering a distance of 150 μm from the edge of the

soma and no significant differences were observed between experimental conditions, regardless of whether neurons were fed with puromycin for 5, 10, or 30 min (**Figure 5B**). Similarly, no significant changes were detected in distal sites ($> 30 \mu\text{m}$ from the soma in these sets of experiments) between DMSO- and $\text{A}\beta$ -treated neurites (**Figure 5C**). Thus, $\text{A}\beta$ treatment does not affect RNA recruitment to neurites. In these experiments, green and red channels corresponding to RNA (SYTO, **Figure 5E**) and protein (puromycin, **Figure 5E**) were binarized in parallel and colocalization between objects in both channels was calculated using the AND function in the FIJI/ImageJ image calculator. The resulting puncta (cyan, **Figure 5E**) were scored in $10 \mu\text{m}$ bins covering a distance of $150 \mu\text{m}$ from the edge of the cell body. No significant differences between DMSO- and $\text{A}\beta$ -treated cells were observed in the distribution of colocalized puncta along neurites (data not shown). Given the high variability, especially in control cells, we did not detect differences between DMSO and $\text{A}\beta$ treatments when focusing on distal sites of Tau-positive neurites either. However, we did observe an accumulation of co-localized foci in $\text{A}\beta$ -treated cells that was not detected in controls when neurons were exposed to puromycin for 30 min compared to the 5-min treatment (**Figure 5D**). We therefore focused on the 30-min puromycin treatment and analyzed the frequency distribution of translating RNAs, measured as the proportion of colocalized puncta. Interestingly, from all translating RNAs detected, half of them were found within the first $30 \mu\text{m}$ proximal to the soma in control cells, whereas this proportion was significantly reduced in $\text{A}\beta$ -treated cells and consequently the percentage of peripheral translating RNAs increased (**Figures 5F,G**). Altogether these results show that $\text{A}\beta$ oligomers increase the sites of localized translation in distal Tau-positive neurites in line with previously published reports (Baleriola et al., 2014; Li and Gotz, 2017; Walker et al., 2018). Thus, the combination of RNA and protein staining techniques followed by image processing and binarization, and object-based colocalization can be successfully used to detect sites of local RNA translation in neurons which might be important to unravel the extent of local changes in early stages of AD and other neurological diseases.

DISCUSSION

Highly polarized cells like neurons heavily rely on the asymmetric distribution of their proteome for their functionality. It was classically thought that proteins that support dendritic and axonal functions are synthesized in the soma and then transported to their target destination at peripheral sites of the neuron. This soma-centric view of protein synthesis has slowly changed over the last two decades and it is now accepted that neurites contain mRNAs and components of the translation machinery and are thus able to produce proteins locally. Local protein synthesis enables neurites (both dendrites and axons) to change their proteome in an acute manner in order to adapt to fast environmental changes. Since the first studies that unambiguously demonstrated the existence of local translation in neurons (Koenig, 1967; Giuditta et al., 1968; Steward and

Levy, 1982; Torre and Steward, 1992; Feig and Lipton, 1993) most work in the field has focused on understanding the role of locally produced proteins in brain physiology. For example, a subset of mRNAs translated in dendrites, which include CamK2a, Calmodulin or Bassoon, is involved in synaptic plasticity (reviewed in Holt et al., 2019). Intra-axonal synthesis of β -actin (Leung et al., 2006), RhoA (Wu et al., 2005), or Par3 (Hengst et al., 2009) is important in growth cone behavior and axon elongation during nervous system development. Proteins involved in mitochondrial function such as LaminB2 (Yoon et al., 2012) or COXIV (Aschrafi et al., 2010) are locally synthesized in axons and contribute to their maintenance in post-developmental stages. However much less is known on the role of local protein synthesis in nervous system pathologies, especially those of the CNS.

Alzheimer's disease (AD), like other neurodegenerative diseases, is characterized by synaptic dysfunction during early stages (Palop and Mucke, 2010). Understanding dynamic early changes in the local proteome (axonal, dendritic or synaptic) is in our view crucial to understand basic pathological mechanisms underlying AD and likely other neurological diseases. Recent work has shown that regulation of intra-axonal protein synthesis induced by $\text{A}\beta_{1-42}$ oligomers, whose accumulation is central to AD, contributes to neurodegeneration (Baleriola et al., 2014). These findings support a model in which retrograde transport of locally produced proteins leads to pathological, transcriptional changes in the neuronal soma. More recently, a link between intra-dendritic translation, and Tau mislocalization and hyperphosphorylation has been found (Kobayashi et al., 2017; Li and Gotz, 2017). Thus, dysregulation of the local translome in neurons might play a more relevant role in AD than previously acknowledged. It is therefore important to know the extent and location of newly synthesized proteins in order to understand early changes in the AD brain.

Despite local translation is finally being accepted by the scientific community, the accurate measurement of this phenomenon is still challenging partly due to the limited amount of proteins that are locally produced, especially in adult axons (Rangaraju et al., 2017). There are other experimental challenges that will be not be discussed herein since the technicalities are beyond the scope of this manuscript. Our own results show that new-synthesized neuritic proteins measured at distal positions ($100\text{--}150 \mu\text{m}$ from the cell nucleus) can be ~ 20 to 30 times less abundant than those measured in the soma in a 30-min time frame (**Figure 2**). Thus, local translation events can be easily overlooked when visualizing *in situ* protein production under the microscope. FUNCAT (Dieterich et al., 2010), and SUnSET (Schmidt et al., 2009) are commonly used techniques in the field of local translation. Both are based on the labeling of newly synthesized proteins, with non-canonical amino acids in the case of FUNCAT or a tRNA analog in the case of SUnSET. In both cases the non-canonical molecules can be fluorescently tagged. Yet when these methods have proven very helpful to analyze the amount of newly synthesized dendritic (Dieterich et al., 2010) and axonal (Wong et al., 2017; Walker et al., 2018) proteins measured as fluorescent intensity in labeled cells, discrete foci of newly produced proteins can come unnoticed unless enhanced.

Some variations of the aforementioned techniques such as Puro-PLA or FUNCAT-PLA have been used to accurately measure discrete translation sites of specific proteins along neurites (Tom Dieck et al., 2015). Both proximity ligation assays (PLA) are based on the spatial coincidence of two antibodies, one that recognizes the recently synthesized polypeptide chain (anti-puromycin in the case of Puro-PLA; anti-biotin for FUNCAT-PLA) and another one that recognizes a specific protein of interest. However, neither PLA approach is useful to analyze all translation foci. Other modifications of SUNSET have been recently used to evaluate overall discrete intra-neuritic and intra-dendritic translation events. For example, co-incubation of neurons with both puromycin and the translation inhibitor emetine prior to fixation prevents the puromycylated polypeptide chain release from the ribosomes. This approach is known as ribopuromycylation (RPM) and it allows the visualization of active polyribosomes in the neuronal soma and along neurites (Graber et al., 2013). Additionally, in puromycin-labeled fixed cells, proximity ligation assay (Puro-PLA) employing a single antibody against puromycin has been used to accurately identify discrete local translation sites in dendrites (Rangaraju et al., 2019). Here we describe a strategy to enhance puromycin hotspots in neurites following SUNSET, based solely on image processing and the assisted quantification of the resulting objects. Our technique does not require the incubation of the cells with any translation inhibitor besides puromycin, and it avoids the processing of the samples for proximity ligation assay, which can be pricy and time consuming.

We first performed edge detection to find discontinuities in our puromycin labeling that could result from a punctate staining arising from discrete positive foci. Instead of using the Find Edges command in FIJI/ImageJ which applies a Sobel edge detector, we used the default 5×5 kernel in the convolver which is a Laplacian edge detector instead. Laplacian operators are very accurate in finding edges in an image but also very sensitive to background noise (Bannister and Larkman, 1995a). We therefore adjusted the minimum and maximum intensities of our micrographs after applying the filter in order to eliminate highlighted pixels outside the area established by the neuronal/axonal markers β III tubulin and Tau (Figure 1; workflow B). We additionally compared the processing workflow between puromycin-positive and puromycin-negative cells and determined that despite possible noise enhancement, positive puncta could be significantly detected over background (Figure 3F, right graph). Image processing with the Laplacian operator highlighted events in the periphery of neurons that could be selected and binarized with the MaxEntropy mask (Figures 1B, 3C, 4D, 5E and Supplementary Figure S1B). Binarization in unprocessed images failed to detect discrete puncta in neurites to the same extent as when images were processed (Supplementary Figure S1).

To determine if our processing method worked in highlighting local events, we evaluated the effect of $A\beta_{1-42}$ oligomers on hippocampal neurites. $A\beta$ oligomers are known to increase puromycin intensity when applied locally to axons, which reflects changes in local protein synthesis (Walker et al., 2018). In our case, we observed similar results in neurites

following bath application of hippocampal neurons with $A\beta$ (Figure 2): the effect elicited by $A\beta$ was visible beyond the canonical ER domain and did not affect the cell body (Figures 2C,G–J). These results are compatible with changes in local translation but they do not address whether actual local sites of protein synthesis are affected by $A\beta$ oligomers. Discrete puncta in distal neuritic sites likely reflect foci of localized translation (Graber et al., 2013; Rangaraju et al., 2019). We quantified discrete puromycin-positive foci in distal neuritic sites in response to $A\beta_{1-42}$ with the particle analyzer after image processing with the convolver (assisted quantification). We observed (1) an enhancement of discrete puromycin staining in both DMSO- and $A\beta$ -treated neurites compared to visual inspection of raw puromycin staining (Figures 3B,C), (2) an enhancement of the effect of $A\beta$ on newly synthesized neuritic proteins compared to controls (Figures 3B,C,I), and (3) a better correlation between the unbiased measurement of puromycin intensity and the number of discrete puromycin-positive sites in processed images (Figure 3H). Altogether these results indicate that binarizing images from puromycin-positive cells after applying a Laplacian edge detector allows the assisted quantification of neuritic translation sites yielding results that resemble those obtained from an unbiased measurement of raw puromycin intensity (Figure 3H). Additionally, our results unravel a previously unreported effect of $A\beta$ oligomers on discrete translation events in neurites (Figures 3E,I).

Our first approach was performed in β III tubulin-positive neurites which correspond to both dendrites and axons. We sought to increase the changes of detecting discrete translation sites since dendrites have been historically reported to have a higher translation capacity than axons (Rangaraju et al., 2017) but because changes in local neuronal translation upon $A\beta$ treatment were first described in axons (Baleriola et al., 2014), we applied the same processing workflow to neurites stained with the axonal marker Tau. Results were very similar to those obtained for β III tubulin-positive neurites when cells were fed with puromycin for 30 min (Figure 4). Shorter exposures to puromycin were also performed in order to minimize the possible detection of newly synthesized proteins diffused from the soma. Puromycin pulses as short as 10–15 min have been successfully used to detect changes in intra-axonal protein synthesis upon acute exposure of axons to $A\beta$ oligomers (Walker et al., 2018). However, we did not observe changes between DMSO- and $A\beta$ -treated cells possibly due to the slow pace of the translation machinery after a 24-h treatment.

In light of our results we addressed whether distal puromycin-positive events in neurites arose from localized RNAs to determine if we were actually measuring local protein synthesis. We applied the processing protocol followed for puromycin staining to SYTO-positive neurites. SYTO RNaselect green fluorescent dye selectively binds neuritic RNA (Figure 5A). We observed that $A\beta$ oligomers did not change the distribution of RNA granules along neurites (Figures 5B,E) nor their amount in distal sites (Figure 5C). These results are compatible with other experiments performed in our laboratory aimed

at labeling neuritic RNAs with alternative techniques (data not shown). Taking advantage of the fact that SYTO-labeled cells were also labeled with puromycin, after binarizing the images corresponding to both stains we applied the AND function in the image calculator which essentially retrieves the colocalization between objects. In our system colocalized objects (cyan, **Figure 5E**) represent sites of actively translating RNAs. We particularly focused on colocalized objects resulting from 30-min puromycin pulses, which were higher than for shorter puromycin exposures (**Figure 5D**). Interestingly, A β_{1-42} increased the proportion of RNA translation in distal sites of Tau-positive neurites, beyond the ER domain. Thus, the combination of RNA and protein staining techniques followed by image processing and binarization, and object-based colocalization can be successfully used to detect sites of local RNA translation in neurons.

Other edge detectors, Laplacian operators distinct to 5×5 matrices or other background subtraction methods can be used depending on the sample requirements and the researcher's criteria. However, the image processing approach described herein has proven very useful to detect discrete events with low pixel intensity, which is the expected characteristic of neuritic local translation sites.

Altogether, this study provides a simple method of quantifying local RNA translation foci using object-recognition and object-based colocalization analyses which allows a better understanding the effect of A β_{1-42} in neurites.

DATA AVAILABILITY STATEMENT

The datasets generated for this study are available on request to the corresponding author.

ETHICS STATEMENT

The animal study was reviewed and approved by Ethics Committee for Animal Care and Use in Research (CEEA) of the University of the Basque Country (UPV/EHU).

REFERENCES

- Aschrafi, A., Natera-Naranjo, O., Gioio, A. E., and Kaplan, B. B. (2010). Regulation of axonal trafficking of cytochrome c oxidase IV mRNA. *Mol. Cell Neurosci.* 43, 422–430. doi: 10.1016/j.mcn.2010.01.009
- Baleriola, J., Walker, C. A., Jean, Y. Y., Crary, J. F., Troy, C. M., Nagy, P. L., et al. (2014). Axonally synthesized ATF4 transmits a neurodegenerative signal across brain regions. *Cell* 158, 1159–1172. doi: 10.1016/j.cell.2014.07.001
- Banker, G., and Goslin, K. (1998). *Culturing Nerve Cells*, 2nd Edn. Cambridge: MIT Press.
- Bannister, N. J., and Larkman, A. U. (1995a). Dendritic morphology of CA1 pyramidal neurons from the rat hippocampus: I. Branching patterns. *J. Comp. Neurol.* 360, 150–160. doi: 10.1002/cne.903600111
- Bannister, N. J., and Larkman, A. U. (1995b). Dendritic morphology of CA1 pyramidal neurones from the rat hippocampus: II. Spine distributions. *J. Comp. Neurol.* 360, 161–171. doi: 10.1002/cne.903600112

AUTHOR CONTRIBUTIONS

JB conceived the project and designed the experiments. MG, MB-U, AB, JI, and JB performed experiments. MG, MB-U, and JB performed data analysis and wrote the manuscript.

FUNDING

JB was supported by two grants from the Spanish Ministry of Science, Innovation and Universities (RYC-2016-19837 start-up funds and SAF2016-76347-R) and start-up funds from the Basque Foundation for Science (IKERBASQUE). MG is a predoctoral fellow funded by the Basque Government. MB-U is a predoctoral fellow funded by the University of the Basque Country (UPV/EHU). AB received funding from the Portuguese Foundation for Science and Technology (FCT) in the context of the FCT funded University of Minho M.D./Ph.D. Program (SFRH/BD/52322/2013).

ACKNOWLEDGMENTS

We thank member of the Neurobiology Lab (Achucarro Basque Center for Neuroscience) for sharing the A β peptides with us.

SUPPLEMENTARY MATERIAL

The Supplementary Material for this article can be found online at: <https://www.frontiersin.org/articles/10.3389/fnins.2020.00547/full#supplementary-material>

FIGURE S1 | Workflows for image processing with or without applying the default convolution kernel (Laplacian filter). Images show the same cells used as examples for the workflow in **Figure 1**. **(B)** Represents the same step by step processing method described **Figure 1B**. **(B')** Corresponds to the same workflow as in **Figure 1B** excluding **step 1** which corresponds to the application of the Laplacian filter to enhance the edges. Both workflows converge in graphs comparing both methods (green line, filter application; red line, no filter) in two experimental conditions (condition 1, blue; condition 2, red). Graphs represent $\text{Log}_2(\# \text{puromycin foci} + 1)$ vs. distance. Scale bars, 50 μm in whole-cell micrographs and 10 μm in straighten neurites.

- Bolton, J. S. (1901). The nervous system and its constituent neurones, designed for the use of practitioners of medicine and of students of medicine and psychology. *Edinb. Med. J.* 10:4.
- Dieterich, D. C., Hodas, J. J., Gouzer, G., Shadrin, I. Y., Ngo, J. T., Triller, A., et al. (2010). In situ visualization and dynamics of newly synthesized proteins in rat hippocampal neurons. *Nat. Neurosci.* 13, 897–905. doi: 10.1038/nn.2580
- Feig, S., and Lipton, P. (1993). Pairing the cholinergic agonist carbachol with patterned Schaffer collateral stimulation initiates protein synthesis in hippocampal CA1 pyramidal cell dendrites via a muscarinic, NMDA-dependent mechanism. *J. Neurosci.* 13, 1010–1021. doi: 10.1523/JNEUROSCI.13-03-01010.1993
- Giuditta, A., Dettbarn, W. D., and Brzin, M. (1968). Protein synthesis in the isolated giant axon of the squid. *Proc. Natl. Acad. Sci. U.S.A.* 59, 1284–1287. doi: 10.1073/pnas.59.4.1284
- Graber, T. E., Hebert-Seropian, S., Khoutorsky, A., David, A., Yewdell, J. W., Lacaille, J. C., et al. (2013). Reactivation of stalled polyribosomes in synaptic

- plasticity. *Proc. Natl. Acad. Sci. U.S.A.* 110, 16205–16210. doi: 10.1073/pnas.1307747110
- Hafner, A. S., Donlin-Asp, P. G., Leitch, B., Herzog, E., and Schuman, E. M. (2019). Local protein synthesis is a ubiquitous feature of neuronal pre- and postsynaptic compartments. *Science* 364:6441. doi: 10.1126/science.aau3644
- Hengst, U., Deglincerti, A., Kim, H. J., Jeon, N. L., and Jaffrey, S. R. (2009). Axonal elongation triggered by stimulus-induced local translation of a polarity complex protein. *Nat. Cell Biol.* 11, 1024–1030. doi: 10.1038/ncb1916
- Holt, C. E., Martin, K. C., and Schuman, E. M. (2019). Local translation in neurons: visualization and function. *Nat. Struct. Mol. Biol.* 26, 557–566. doi: 10.1038/s41594-019-0263-5
- Jung, H., Gkogkas, C. G., Sonenberg, N., and Holt, C. E. (2014). Remote control of gene function by local translation. *Cell* 157, 26–40. doi: 10.1016/j.cell.2014.03.005
- Jung, H., Yoon, B. C., and Holt, C. E. (2012). Axonal mRNA localization and local protein synthesis in nervous system assembly, maintenance and repair. *Nat. Rev. Neurosci.* 13, 308–324. doi: 10.1038/nrn3210
- Kobayashi, S., Tanaka, T., Soeda, Y., Almeida, O. F. X., and Takashima, A. (2017). Local somatodendritic translation and hyperphosphorylation of tau protein triggered by AMPA and NMDA receptor stimulation. *EBioMedicine* 20, 120–126. doi: 10.1016/j.ebiom.2017.05.012
- Koenig, E. (1967). Synthetic mechanisms in the axon. IV. In vitro incorporation of [³H]precursors into axonal protein and RNA. *J. Neurochem.* 14, 437–446. doi: 10.1111/j.1471-4159.1967.tb09542.x
- Leung, K. M., van Horck, F. P., Lin, A. C., Allison, R., Standart, N., and Holt, C. E. (2006). Asymmetrical beta-actin mRNA translation in growth cones mediates attractive turning to netrin-1. *Nat. Neurosci.* 9, 1247–1256. doi: 10.1038/nn1775
- Li, C., and Gotz, J. (2017). Somatodendritic accumulation of Tau in Alzheimer's disease is promoted by Fyn-mediated local protein translation. *EMBO J.* 36, 3120–3138. doi: 10.15252/embj.201797724
- Palop, J. J., and Mucke, L. (2010). Amyloid-beta-induced neuronal dysfunction in Alzheimer's disease: from synapses toward neural networks. *Nat. Neurosci.* 13, 812–818. doi: 10.1038/nn.2583
- Quintela-Lopez, T., Ortiz-Sanz, C., Serrano-Regal, M. P., Gaminde-Blasco, A., Valero, J., Baleriola, J., et al. (2019). Abeta oligomers promote oligodendrocyte differentiation and maturation via integrin beta1 and Fyn kinase signaling. *Cell Death Dis.* 10:445. doi: 10.1038/s41419-019-1636-8
- Rangaraju, V., Lauterbach, M., and Schuman, E. M. (2019). Spatially stable mitochondrial compartments fuel local translation during plasticity. *Cell* 7:e15. doi: 10.1016/j.cell.2018.12.013
- Rangaraju, V., Tom Dieck, S., and Schuman, E. M. (2017). Local translation in neuronal compartments: how local is local? *EMBO Rep.* 18, 693–711. doi: 10.15252/embr.201744045
- Rutkevich, L. A., and Williams, D. B. (2011). Participation of lectin chaperones and thiol oxidoreductases in protein folding within the endoplasmic reticulum. *Curr. Opin. Cell Biol.* 23, 157–166. doi: 10.1016/j.ccb.2010.10.011
- Savas, J. N., Ma, B., Deinhardt, K., Culver, B. P., Restituito, S., Wu, L., et al. (2010). A role for huntington disease protein in dendritic RNA granules. *J. Biol. Chem.* 285, 13142–13153. doi: 10.1074/jbc.M110.114561
- Schmidt, E. K., Clavarino, G., Ceppi, M., and Pierre, P. (2009). SUNSET, a nonradioactive method to monitor protein synthesis. *Nat. Methods* 6, 275–277. doi: 10.1038/nmeth.1314
- Steward, O., and Levy, W. B. (1982). Preferential localization of polyribosomes under the base of dendritic spines in granule cells of the dentate gyrus. *J. Neurosci.* 2, 284–291. doi: 10.1523/JNEUROSCI.02-03-00284.1982
- Terenzio, M., Koley, S., Samra, N., Rishal, I., Zhao, Q., Sahoo, P. K., et al. (2018). Locally translated mTOR controls axonal local translation in nerve injury. *Science* 359, 1416–1421. doi: 10.1126/science.aan1053
- Tom Dieck, S., Kochen, L., Hanus, C., Heumuller, M., Bartnik, I., Nassim-Assir, B., et al. (2015). Direct visualization of newly synthesized target proteins in situ. *Nat. Methods* 12, 411–414. doi: 10.1038/nmeth.3319
- Torre, E. R., and Steward, O. (1992). Demonstration of local protein synthesis within dendrites using a new cell culture system that permits the isolation of living axons and dendrites from their cell bodies. *J. Neurosci.* 12, 762–772. doi: 10.1523/JNEUROSCI.12-03-00762.1992
- Walker, C. A., Randolph, L. K., Matute, C., Alberdi, E., Baleriola, J., and Hengst, U. (2018). Abeta1-42 triggers the generation of a retrograde signaling complex from sentinel mRNAs in axons. *EMBO Rep.* 19:e45435. doi: 10.15252/embr.201745435
- Wong, H. H., Lin, J. Q., Strohl, F., Roque, C. G., Cioni, J. M., Cagnetta, R., et al. (2017). RNA docking and local translation regulate site-specific axon remodeling in vivo. *Neuron* 85:e858. doi: 10.1016/j.neuron.2017.07.016
- Wu, K. Y., Hengst, U., Cox, L. J., Macosko, E. Z., Jeromin, A., Urquhart, E. R., et al. (2005). Local translation of RhoA regulates growth cone collapse. *Nature* 436, 1020–1024. doi: 10.1038/nature03885
- Yarmolinsky, M. B., and Haba, G. L. (1959). Inhibition by puromycin of amino acid incorporation into protein. *Proc. Natl. Acad. Sci. U.S.A.* 45, 1721–1729. doi: 10.1073/pnas.45.12.1721
- Yoon, B. C., Jung, H., Dwivedy, A., O'Hare, C. M., Zivraj, K. H., and Holt, C. E. (2012). Local translation of extranuclear lamin B promotes axon maintenance. *Cell* 148, 752–764. doi: 10.1016/j.cell.2011.11.064

Conflict of Interest: The authors declare that the research was conducted in the absence of any commercial or financial relationships that could be construed as a potential conflict of interest.

Copyright © 2020 Gamarra, Blanco-Urrejola, Batista, Imaz and Baleriola. This is an open-access article distributed under the terms of the Creative Commons Attribution License (CC BY). The use, distribution or reproduction in other forums is permitted, provided the original author(s) and the copyright owner(s) are credited and that the original publication in this journal is cited, in accordance with accepted academic practice. No use, distribution or reproduction is permitted which does not comply with these terms.